



Statistical analysis of process parameters and multi-objective optimization in wire electrical discharge machining of Al 7075 using weight-based constrained algorithm

Kingshuk Mandal¹ · Mukandar Sekh² · Dipankar Bose³ · Souren Mitra¹ · Soumya Sarkar¹

Received: 26 September 2022 / Accepted: 12 November 2022 / Published online: 29 November 2022
© The Author(s), under exclusive licence to Springer-Verlag France SAS, part of Springer Nature 2022

Abstract

In the present work, the influence of four significant wire electrical discharge machining (WEDM) parameters, such as pulse duration (T_{on}), pulse interval (T_{off}), servo voltage (S_v) and wire tension (W_t) has been studied on cutting velocity (V_c), diagonal dimensional deviation (D_v) and surface roughness (R_a). Signal-to-noise ratio and analysis of variance are used to analyse the effects of four cutting parameters. An entropy weight method is used to determine the objective weights. An integrated weight-based multi-constrained optimization technique is employed to find the optimal solutions for multiple responses. Optimal solutions show that diagonal dimension deviation (D_v) ranges from 0.128 to 0.241 mm and surface roughness (R_a) ranges from 1.058 to 3.457 μ m for a wide range of cutting velocity (V_c). It is also found that the weight-based Pareto results are improved by 10.5% (for cutting velocity) 28.3% (for dimensional accuracy) and 13.7% (for surface finish) compared to the general Pareto results. Additionally, an important aspect, radial overcut (δ) is measured to predict the linear error present in the workpiece. Finally, CCI and SEM analyses have been carried out to evaluate the surface characteristics of the machined surface. It is evident from the machined surface that the surface is full of small craters, micro-holes, re-solidified materials and recast globules.

Keyword WEDM · Al 7075 · EWM · Diagonal dimensional deviation · Radial overcut

1 Introduction

Due to the advancement of technology, conventional materials are being gradually replaced by advanced alloys. In the last decade of their first introduction, high conductive materials, especially aluminium alloys, are at the forefront of engineering materials. Recently, several researchers have focused on them because of their distinctive and attractive qualities [1–5]. Al 7075 is a new generation light metal alloy. It becomes extensively important in present day production industries due to its high capability to resist temperature and stress corrosion cracking [6]. Additionally, it is also known as

an advanced alloy that widely used in different manufacturing industry to make intricate shapes with desired accuracy [7]. Initially, it was considered as an alternative solution to iron and titanium alloy for high temperature applications [8–10]. Later on, it becomes non-dominated in structural applications and the aviation industry [11]. The major applications of this alloy are in turbine industries, heat exchangers, armour, automobile engine cylinders and chemical industries etc. [12, 13]. The material has outstanding mechanical properties. Therefore, machining the material is difficult with traditional techniques [14]. Wire electro discharge machining (WEDM) is a potential solution to effectively machine this material. It is an economical process extensively used in manufacturing industries [15, 16]. In WEDM, material removal takes place by a series of isolated sparks between the tool electrode (wire) and the workpiece submerged in a liquid dielectric medium. Initially, electrical discharge energy is converted into thermal energy to melt and vaporized minute amounts of material, which are then propelled and waved out by the external flow of dielectric [17–19]. This dielectric liquid is also used as a coolant to defeat the heat developed

✉ Kingshuk Mandal
mandal.kingshuk1@gmail.com

¹ Production Engineering Department, Jadavpur University, Kolkata 700032, India

² Mechanical Engineering Department, Aliah University, Kolkata 700160, India

³ Mechanical Engineering Department, NITTTR-Kolkata, Kolkata 700106, India

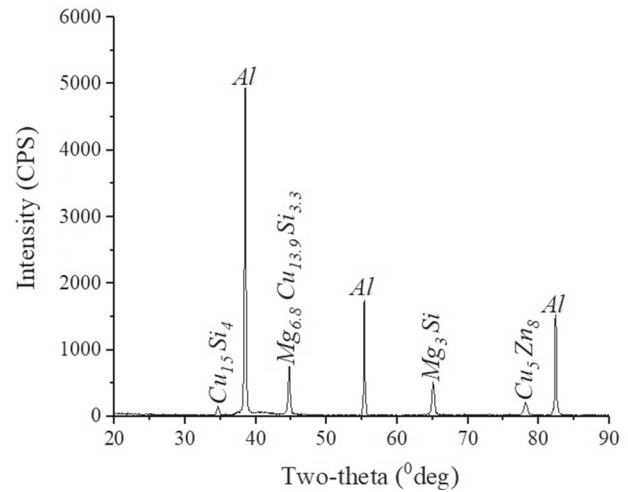
Table 1 Chemical compositions of Al 7075 alloy

Compositions	Al	Zn	Mg	Cu	Si	Balance
Weight %	90.00	4.35	3.17	2.23	0.14	0.11

in the machining zone as well as remove the cutting materials. The final aim of the WEDM process is to accomplish an exact and proficient output. Generally, it can be achieved by considering the relationship between the number of features affecting the process and obtaining the optimal machining conditions [20, 21].

Process parameter selection is a critical task in WEDM. The parameter selections mainly depend upon the operator's skills and the manual provided by the machine tool manufacturer [22]. Some process parameters are highly connected to each other. This means that the same parameter settings may not be effective to achieve a high production rate, good surface quality, and high dimensional accuracy [23]. Due to the intricacy of the process, selecting appropriate parameters and their settings to obtain the best cutting condition is extremely difficult [24]. Therefore, customized parameter settings for optimal machining of materials are needed. For that purpose, many efforts have been made in WEDM. Conventionally used stainless steel and stainless-clad steel are not the same type of material. Stainless-clad steel is an advanced layered composite that is widely used in modern manufacturing industries. Therefore, parameter settings to machine this material are different from those for conventional steel and are not available in the machine tool manufacturer's manuals [25–27]. Similarly, customized parameter settings are needed to machine advanced materials like Ti6Al4V, NIMONIC, Inconel, etc. On the other hand, parameter settings may vary when deionized water is replaced by a powder mix dielectric [28–30]. In such circumstances, general parameter settings cannot effectively machine the materials. For that purpose, modified parameter settings are needed to increase the production rate and machining efficiency.

From the review of past literature, it is found that limited research has been carried out in WEDM of Al 7075-based MMCs [31–33]. A few research works are available on the Al 7075 alloy [34, 35]. Most of the previous researchers have concentrated on achieving the highest MRR and linear dimensional accuracy by controlling the variable process parameters [36–38]. Some researchers have investigated the surface characteristics and tribological behaviour of WEDM surfaces on different materials [39–41]. Limited research is available in WEDM to control the wire lag during corner cutting. So far, no such research has been reported on diagonal accuracy improvement and radial overcut prediction in WEDM of Al 7075. Additionally, diagonal accuracy and cutting speed improvement in WEDM of this alloy is not

**Fig. 1** XRD pattern of the Al 7075 alloy

yet fully solved. The present research explores the machinability and optimal cutting of Al 7075 in WEDM. In this concern, the entropy weight method (EWM) is employed to find out the appropriate weight of responses. Later, calculated entropy weights are used in the constrained Pareto algorithm to obtain better optimal solutions. In this work, four important performances are considered: cutting velocity, diagonal dimensional deviation, surface roughness and radial overcut.

2 Experimentations

2.1 Material

Chemical compositions and weight percentages of the workpiece material are given in Table 1. At room temperature, X-ray diffraction (XRD) of the material is performed to identify the various phases that exist in it. Figure 1 shows the XRD pattern of Al 7075. Other common and significant properties of this material are density of 2.81 g/cm³, melting point of 635 °C, ultimate tensile strength of 572 MPa and hardness of 150 BHN, thermal conductivity of 170 W/m K and electrical conductivity of 19.2 mega-Siemens/m.

3 Experimental procedure

A schematic diagram of the wire electrical discharge machining (WEDM) process is shown in Fig. 2. In this work, EX-40

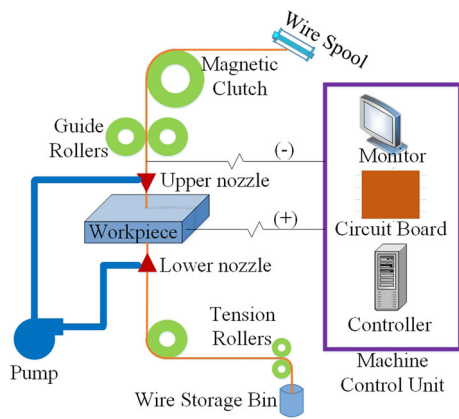


Fig. 2 Schematic diagram of WEDM process

WEDM system is used to conduct the experiments. A photographic view of the EX-40 WEDM table unit is shown in Fig. 3a. Schematic representation of a slot produced by the wire electrode is shown in Fig. 3b. Al 7075 plate is mounted on the worktable and a specimen of 8 mm (length) × 8 mm (width) × 25 mm (thickness) is sliced from the uncut workpiece. Four variable process parameters are selected as pulse duration (T_{on}), pulse interval (T_{off}), servo voltage (S_v) and wire tension (W_t). Experiments have been carried out

in deionized water with a conductivity setting of 12 mho and an electrode of coated brass wire with a diameter of 250 μ m. Some other process parameters, such as wire feed rate (10 m/min), flushing pressure (8 kgf/cm²), open circuit voltage (50 V) and servo sensitivity (6) remain constant during experiments. These process parameters and their range have been selected on the basis of the existing literature, pilot experimentation, manufacturer’s manual, and machine capability. After the selection of process parameters and their levels, the final set of experiments has been conducted. In the final set of experiments, each experiment is conducted repeatedly. It is observed that the same experiment, with the same setup, produced approximately the same results. Selected independent input parameters and their levels are indicated in Table 2. In this work, four important performance characteristics are considered: cutting velocity (V_c : mm/min), diagonal dimensional deviation (D_v : mm), surface roughness (R_a : μ m) and radial overcut (δ : μ m).

4 Measurement of responses

Cutting velocity (V_c) is captured from the monitor of the machine. Surface roughness (R_a) is measured using a contact type surface roughness tester (Mitutoyo: SJ 400). An average

Fig. 3 a Machining table unit of EX-40 WEDM system, b schematic representation of the slot produced by wire electrode

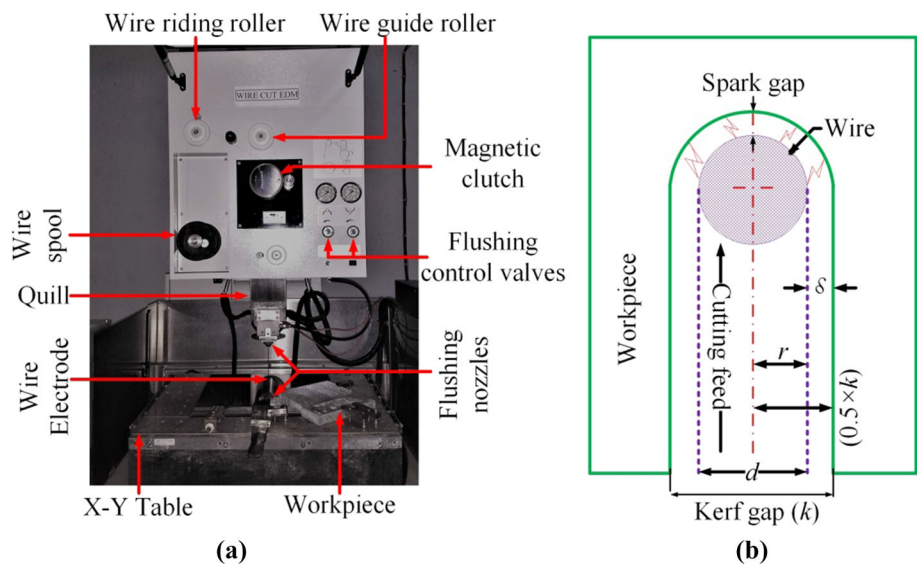
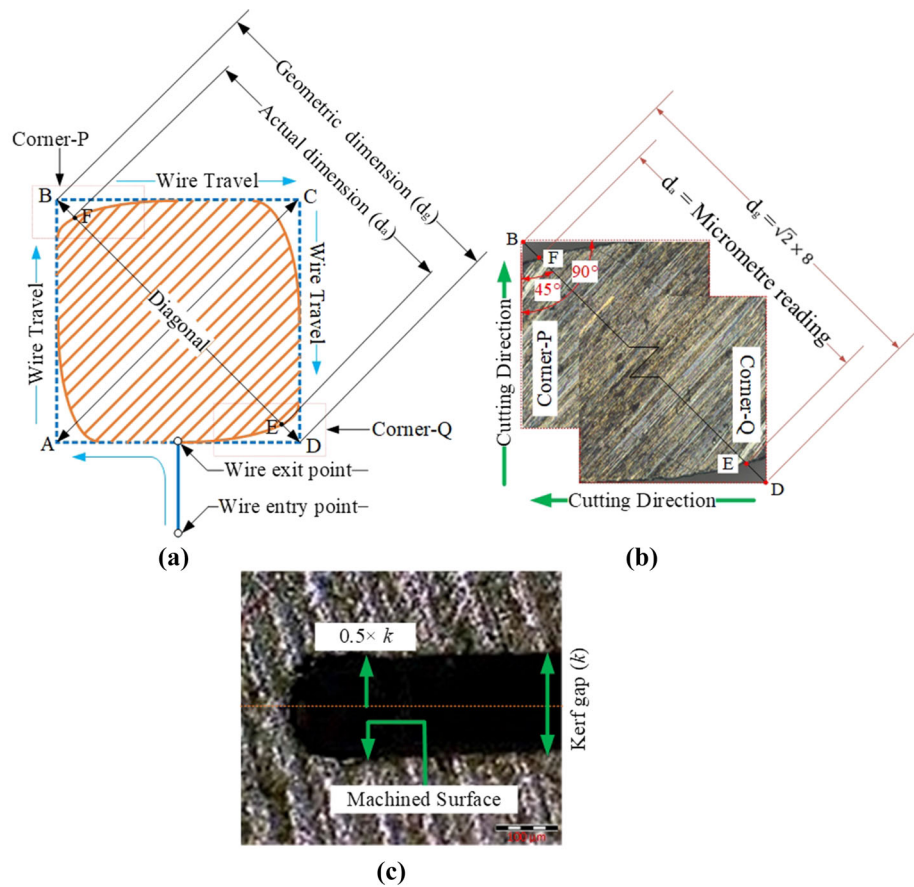


Table 2 Units, levels and notations of process parameters

Input parameters	Notations	Units	Levels		
			Low (1)	Medium (2)	High (3)
Pulse duration	T_{on}	μ s	0.1	0.4	0.7
Pulse interval	T_{off}	μ s	15	25	35
Servo voltage	S_v	volt	20	30	40
Wire tension	W_t	kg	0.5	0.8	1.1

Fig. 4 **a** Schematic representation of diagonal dimensional deviation, **b** microscopic image of diagonal dimensional deviation measurement, **c** radial overcut measurement



of cutting velocity and surface roughness is calculated from the collected raw data. Diagonal dimensional deviation (D_v) and radial overcut (δ) are measured using a high-precision digimatic Mitutoyo micrometre (Least count = $0.1 \mu\text{m}$). Here, the diagonal dimensional deviation is the difference between the theoretical and actual diagonal length of the profile. Similarly, radial overcut is the difference between half of the kerf gap ($k/2$) and wire radius (r). Figure 4a, b shows the schematic diagram and measurement technique of diagonal dimensional deviation. Figure 4c represents the microscopic image of radial overcut measurement. The diagonal dimensional deviation and radial overcut are calculated as follows (Given in Eqs. 1, 2):

$$\text{Diagonal dimensional deviation } (D_v) = d_g - d_a \quad (1)$$

where d_g = theoretical diagonal length and d_a = actual diagonal length.

$$\text{Radial overcut } (\delta) = \frac{k}{2} - \frac{d}{2} = \left(\frac{k}{2} - r \right) \quad (2)$$

where k = kerf gap, d = wire diameter and r = wire radius.

5 Theory of experimental design

Design of experiments (DOE) is an efficient approach to conduct experiments in a regular manner. It gives appropriate knowledge for better understanding of the relationship between process parameters and performance characteristics [42, 43]. Generally, DOE is categorized as full factorial design or fractional factorial design [44]. In this study, an L_{27} fractional factorial design is used to conduct the experiments. In this method, input and output parameters are assigned in the columns and numbers of experimental runs are allotted in the rows. Table 3 shows the experimental design matrix. The experimental results are then used to model the process and calculate the objective weights.

In the Taguchi design technique, signal-to-noise (S/N) ratio is used to govern the performance characteristics of the process variables. In this method, three different performance characteristics known as higher-the-better, lower-the-better and nominal-the-better are commonly used [45]. Higher cutting velocity is always desirable to get better productivity in any process. So, cutting velocity is selected as larger-the-better kind of problem. On the other hand, diagonal dimensional deviation, surface roughness and radial overcut are defined the level of accuracy and quality features

Table 3 Design matrix for process factors and response criteria

Sl. no.	Input factors				Responses						
	Pulse duration (T _{on} : μs)	Pulse interval (T _{off} : μs)	Servo voltage (S _v : volt)	Wire tension (W _t : kg)	Cutting velocity (V _c : mm/min)	Diagonal dimensional deviation (D _v : mm)	Surface roughness (R _a : μm)				Radial overcut (δ: μm)
							Data-1	Data-2	Data-3	Std. Dev	
1	0.1	15	20	0.5	1.67	0.157	1.339	1.121	1.263	0.111	20
2	0.1	15	20	0.5	1.64	0.152	1.107	1.265	1.339	0.119	19
3	0.1	15	20	0.5	1.69	0.155	1.353	1.379	1.32	0.030	17
4	0.1	25	30	0.8	1.13	0.142	2.422	2.626	2.539	0.102	14
5	0.1	25	30	0.8	1.15	0.148	2.512	2.546	2.679	0.088	16
6	0.1	25	30	0.8	1.12	0.144	2.587	2.451	2.654	0.103	12
7	0.1	35	40	1.1	0.66	0.123	3.221	3.149	3.035	0.094	11
8	0.1	35	40	1.1	0.68	0.127	3.232	3.164	3.345	0.091	13
9	0.1	35	40	1.1	0.65	0.125	3.404	3.512	3.305	0.104	15
10	0.4	15	30	1.1	3.14	0.169	2.316	2.221	2.111	0.103	22
11	0.4	15	30	1.1	3.11	0.165	2.421	2.221	2.336	0.100	20
12	0.4	15	30	1.1	3.19	0.167	2.261	2.337	2.154	0.092	19
13	0.4	25	40	0.5	2.22	0.192	3.827	3.644	3.764	0.093	26
14	0.4	25	40	0.5	2.19	0.194	3.469	3.551	3.651	0.091	28
15	0.4	25	40	0.5	2.24	0.196	3.769	3.914	3.681	0.118	27
16	0.4	35	20	0.8	2.67	0.178	4.356	4.531	4.415	0.089	21
17	0.4	35	20	0.8	2.71	0.173	4.658	4.601	4.505	0.077	23
18	0.4	35	20	0.8	2.73	0.175	4.592	4.776	4.654	0.094	24
19	0.7	15	40	0.8	5.83	0.267	2.714	2.677	2.541	0.091	34
20	0.7	15	40	0.8	5.88	0.264	2.637	2.553	2.442	0.098	33
21	0.7	15	40	0.8	5.79	0.261	2.773	2.591	2.697	0.091	31
22	0.7	25	20	1.1	5.24	0.215	4.017	4.227	4.109	0.105	28
23	0.7	25	20	1.1	5.30	0.211	4.156	3.985	4.118	0.090	26
24	0.7	25	20	1.1	5.19	0.217	4.185	4.149	4.107	0.039	27
25	0.7	35	30	0.5	4.28	0.248	4.847	4.812	4.672	0.093	29
26	0.7	35	30	0.5	4.32	0.246	4.927	4.780	4.931	0.086	27
27	0.7	35	30	0.5	4.27	0.242	4.635	4.859	4.799	0.116	25

of the product. Therefore, diagonal dimensional deviation, surface roughness and radial overcut must be on the lower side. So, diagonal dimensional deviation, surface roughness and radial overcut are considered as smaller-the-better kinds of problems. Signal-to-noise (S/N) ratio for three different performance characteristics are expressed as follows (Eqs. 3–5):

$$\text{Higher the better : S/N ratio} = -10 \log \left\{ \frac{1}{n} \sum_{i=1}^n \left(\frac{1}{y_i^2} \right) \right\} \tag{3}$$

$$\text{Lower the better : S/N ratio} = -10 \log \left\{ \frac{1}{n} \sum_{i=1}^n (y_i^2) \right\} \tag{4}$$

$$\text{Nominal the better : S/N ratio} = 10 \log \left\{ \frac{\hat{y}^2}{s^2} \right\} \tag{5}$$

where y_i is the experiential response, \hat{y} is the mean, s is the variance and n is the number of experimental runs.

6 Results and discussion

6.1 Analysis of the process parameters based on Taguchi methodology

The input parameters and their levels are listed in Table 2. Based upon the experimental design, twenty-seven experiments (given in Table 3) have been carried out on Al 7075 workpiece in order to find out the effects of process

Fig. 5 SN ratio plot of the process parameters in different levels **a** cutting speed, **b** diagonal dimensional deviation, **c** surface roughness, **d** radial overcut

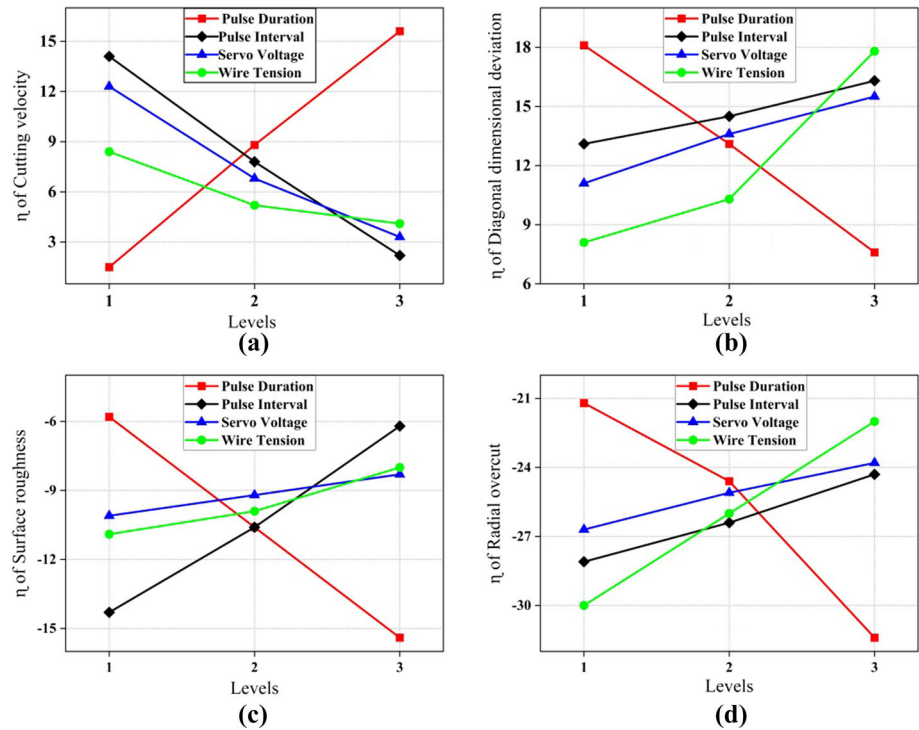


Table 4 Analysis of cutting velocity data

Source	<i>df</i>	Adj SS	Adj MS	F-value	<i>P</i> value
Regression	8	78.5058	9.81323	8773.41	0.000
T_{on}	1	0.4971	0.49713	444.45	0.000
T_{off}	1	0.4836	0.48357	432.33	0.000
S_v	1	0.2950	0.29505	263.78	0.001
W_t	1	0.1551	0.15511	164.50	0.000
T_{on}^2	1	1.2120	1.21200	1083.58	0.000
T_{off}^2	1	0.2578	0.25782	285.80	0.000
S_v^2	1	0.1347	0.13470	109.83	0.004
W_t^2	1	0.0444	0.04436	65.49	0.000
Error	18	0.0201	0.00112		
Total	26	78.5259			
S	R^2	R^2 (adj)	R^2 (pred)		
	0.0134	99.97%	99.96%	98.94%	

parameters on cutting velocity (V_c), diagonal dimensional deviation (D_v), surface roughness (R_a) and radial overcut (δ). Figure 5a–d describes the effects of process parameters at various levels. Based upon the experimental findings analysis of variance (ANOVA) has been carried out to estimate the model accuracy and determine the relative significance of each process parameter. The analysis has been carried out at 95% confidence level. The *P* value of aforementioned factors (i.e. T_{on} , T_{off} , S_v and W_t) and their squared terms (i.e. T_{on}^2 , T_{off}^2 , S_v^2 and W_t^2) are less than the specified α -value (< 5%). From the ANOVA of cutting velocity data as shown

in Table 4, it is observed that pulse duration, pulse interval, servo voltage and wire tension play a significant role to determine the cutting velocity. Similarly, from the analysis of diagonal dimensional deviation data in Table 5, it is found that pulse duration and wire tension are important process parameters. Pulse interval and servo voltage are also influencing factors but their significance is low as compared to pulse duration and wire tension to determine the diagonal dimensional deviation. From the Table 6 it is observed that most important factor for surface roughness values are pulse duration and pulse interval. On the other hand, from

Table 5 Analysis of diagonal dimensional deviation data

Source	<i>df</i>	Adj SS	Adj MS	F-value	<i>P</i> value
Regression	8	0.052036	0.006505	949.31	0.000
T_{on}	1	0.000517	0.000517	71.67	0.000
T_{off}	1	0.000183	0.000183	26.67	0.000
S_v	1	0.000088	0.000088	11.14	0.009
W_t	1	0.000432	0.000432	63.10	0.000
T_{on}^2	1	0.000946	0.000946	138.04	0.000
T_{off}^2	1	0.000307	0.000307	45.61	0.005
S_v^2	1	0.000130	0.000130	24.32	0.032
W_t^2	1	0.000763	0.000763	111.38	0.000
Error	18	0.000123	0.000007		
Total	26	0.052159			
S	R^2	R^2 (adj)	R^2 (pred)		
0.0026	99.76%	99.66%	98.07%		

Table 6 Analysis of surface roughness data

Source	<i>df</i>	Adj SS	Adj MS	F-value	<i>P</i> value
Regression	8	32.5239	4.06549	547.35	0.000
T_{on}	1	2.6461	2.64606	356.25	0.000
T_{off}	1	1.7215	1.72147	231.77	0.000
S_v	1	0.2201	0.22011	21.71	0.007
W_t	1	0.1903	0.19035	17.05	0.031
T_{on}^2	1	0.9659	0.96588	130.04	0.000
T_{off}^2	1	0.6281	0.62813	84.57	0.000
S_v^2	1	0.1237	0.12370	10.84	0.021
W_t^2	1	0.0808	0.08085	5.11	0.046
Error	18	0.0337	0.00743		
Total	26	32.6576			
S	R^2	R^2 (adj)	R^2 (pred)		
0.0361	99.59%	98.41%	97.38%		

the analysis of the radial overcut data are given in Table 7, it is observed that pulse duration and wire tension are most crucial factors to determine the radial overcut. Pulse interval and servo voltage also have moderate effects on radial overcut but their impacts are low in respect of pulse duration and wire tension. From the S/N ratio plot, it is observed that the cutting velocity increases as the pulse duration increases and decreases as the pulse interval, servo voltage, and wire tension are increased (shown in Fig. 5a). Figure 5b shows that the diagonal dimensional deviations significantly increase with an increase in pulse duration and strongly decrease as the wire tension increase. It is also observed that the diagonal dimensional deviation decreases as the pulse interval and servo voltage increase. However, it is observed that the impact of servo voltage on diagonal dimensional deviation is low as compared to the other parameters. Surface roughness

is significantly decreased as the pulse interval, servo voltage and wire tension increase (shown in Fig. 5c). Similarly, radial overcut (δ) increases as the pulse duration increases but effectively decreases as the pulse interval, servo voltage and wire tension increase (shown in Fig. 5d).

Cutting velocity significantly increases as the pulse duration increases and decreases when the pulse interval increases (shown in Fig. 5a). The fact is that cutting velocity is proportionate with the discharge energy contained in each pulse. It not only depends upon the discharge energy per pulse but also on applied power, energy rate and crater per volume. As the pulse duration increases and the pulse interval decreases, power and energy per pulse in a given time period increase. This increase in discharge energy per pulse produced more heat which increases the material evaporation rate. This discharge energy per pulse and the applied power decide the

Table 7 Analysis of radial overcut data

Source	<i>df</i>	Adj SS	Adj MS	F-value	<i>P</i> value
Regression	8	1038.07	129.759	50.05	0.000
Ton	1	84.52	84.524	32.60	0.000
Toff	1	26.01	26.013	10.24	0.004
Sv	1	21.22	21.218	8.76	0.019
Wt	1	61.85	61.853	24.71	0.000
T_{on}^2	1	39.80	39.796	13.78	0.008
T_{off}^2	1	15.46	15.463	6.18	0.028
S_v^2	1	8.02	8.019	3.61	0.034
W_t^2	1	25.35	25.352	10.06	0.009
Error	18	2.67	0.0393		
Total	26	1084.74			
S	R ²	R ² (adj)	R ² (pred)		
0.0611	99.10%	97.29%	96.02%		

material removal rate (MRR). Therefore, an increase in pulse duration i.e. power and energy, enhance the material removal rate and subsequently increases the cutting velocity. Similarly, lower servo voltage always gives a higher cutting velocity. This is happening due to better utilization of discharge energy per spark. As the servo voltage increases, the gap between electrodes (i.e. inter-electrode gap: IEG) also increases. As the IEG increases, the utilization of energy per pulse in the machining zone decreases and cutting velocity is considerably reduced.

The effects of pulse duration, pulse interval, servo voltage and wire tension on diagonal dimensional deviation are presented in Fig. 5b. It is perceived that the diagonal dimensional deviation significantly increases as the pulse duration increases and decreases as the pulse interval increases. This is happening due to increasing the number of discharges in a given pulse cycle. With an increase in pulse duration, total energy contained in each cycle is increasing so the cutting speed is increased. Due to the higher cutting speed, transverse vibration in the wire electrode is increased and reduced the diagonal accuracy. On the other hand, due to longer pulse duration, gap force is generated in the inter electrode gap (IEG) which promotes the diagonal deviation. This wire vibration and gap force are the deciding factors to determine the diagonal dimensional deviation and linear error. Diagonal deviation and linear error decreases as the wire tension increases. The fact is that the wire electrode becomes more straight and stable to maintain the vertical position. As a result, gap force and vibration present in the electrode decrease, which enhances the dimensional accuracy. Diagonal dimensional deviation decreases as the servo voltage increases. The utilization of energy per pulse decreases as the servo voltage increases. Due to the less utilization of

energy, wire vibration and spark gap force becomes low and improve the diagonal accuracy.

It is anticipated that from Fig. 5c, surface roughness will increase as the pulse duration increases. On the other hand, surface roughness decreases as the pulse interval, servo voltage, and wire tension are increased. The longer the pulse duration and the shorter the pulse interval, the more power and energy will be conveyed to the machining zone and make a more stable plasma channel. Due to this aggressive pulse parameter setting, energy per pulse i.e. magnitude of discharge energy is increased. For that reason, intense sparking is visualised in the machining zone. This high discharge energy introduces a localized heat flux into the work surface that produced strong melting and vaporization of the material. As a result, the formation of craters, voids and recast globules on the surface increases, which in turn increases the surface roughness. On the other hand, surface finish improves when servo voltage is increased. At higher servo voltage, the gap between the electrodes increases and utilization of energy per pulse decreases. For that reason, presence of craters, recast globules and voids is comparatively less on the machined surface.

As shown in Fig. 5d, the radial overcut increases as the pulse duration increases and decreases as the pulse interval, servo voltage and wire tension increase. The fact is that pulse duration is a key factor to increase the discharge energy and power. Increasing the pulse duration increases the power and discharge energy, which increases the rate of material removal or cutting velocity. With the increase in pulse duration and decrease in pulse interval, more powerful discharge takes place in the machining zone. This high discharge energy in the cutting area produced intense localized heat and removes large amount of material and causes the

widening of the machine slot. The machining slot is generated due to the erosion of material from the workpiece along the cutting direction. This generated machining slot is known as kerf width or kerf gap (k). On the other hand, this kerf gap (k) is the summation of wire diameter (d) and total overcut (2δ). As the MRR increases with an increase in pulse duration, the kerf gap and overcut increase. It is also observed that wire tension plays a pivotal role to determine the radial overcut. Radial overcut decreases as the wire tension increase. As the wire tension increases, electrode (wire) try to maintain the original position (i.e. vertical position) which reduced the lateral and longitudinal vibrations in the wire. For that reason, uniform sparking takes place in the IEG and avoids irregular erosion of material from the sidewall. Therefore, kerf width as well as radial overcut decreases as the wire tension increases.

7 Development of statistical models based on experimental results

A model is developed to establish the relationship between independent decision variables and responses in terms of a mathematical equation. In this study, a non-linear regression technique is used to correlate the independent inputs and outputs. The functional equation of the quadratic model can be written as:

$$y(V_c, D_v, R_a, \delta) = f(T_{on}, T_{off}, S_v, W_t) \tag{6}$$

where V_c, D_v, R_a and δ are the response factors, namely cutting velocity, diagonal dimensional deviation, surface roughness and radial overcut. T_{on}, T_{off}, S_v and W_t are the independent process parameters known as pulse duration, pulse interval, servo voltage and wire tension.

The quadratic model of four parameters with their coefficient can be expressed as-

$$y(V_c, D_v, R_a, \delta) = \mu_0 + (\mu_1 T_{on} + \mu_2 T_{off} + \mu_3 S_v + \mu_4 W_t) + (\mu_{11} T_{on}^2 + \mu_{22} T_{off}^2 + \mu_{33} S_v^2 + \mu_{44} W_t^2) \tag{7}$$

where μ_0 is the constant term (coefficient) in the model. μ_1, μ_2, μ_3 and μ_4 are the linear coefficient and $\mu_{11}, \mu_{22}, \mu_{33}$ and μ_{44} are the coefficient of squared term.

Coefficients are calculated using the Minitab-20 software package. A final model is developed after determining the coefficient of each term. The calculated coefficients are

replaced in Eq. 5 and the final form of equations are as follows:

$$y_1 = V_c = 2.565 + 2.618T_{on} - 0.14289T_{off} - 0.13367S_v + 6.751W_t + 4.994T_{on}^2 + 0.001861T_{off}^2 + 0.001978S_v^2 - 3.914W_t^2 \tag{8}$$

$$y_2 = D_v = 0.1403 + 0.05469T_{on} - 0.002778T_{off} - 0.000689S_v + 0.1518W_t + 0.1395T_{on}^2 + 0.000042T_{off}^2 + 0.000022S_v^2 - 0.1253W_t^2 \tag{9}$$

$$y_3 = R_a = -2.127 + 6.04T_{on} + 0.2696T_{off} - 0.0349S_v + 0.136W_t - 4.458T_{on}^2 - 0.003236T_{off}^2 + 0.000478S_v^2 - 0.132W_t^2 \tag{10}$$

$$y_4 = \delta = 36.84 + 34.14T_{on} - 0.011T_{off} - 1.761S_v + 9.9W_t - 14.2T_{on}^2 - 0.00278T_{off}^2 + 0.03056S_v^2 - 10.49W_t^2 \tag{11}$$

Another set of verification experiments is conducted to validate the developed models. The confirmatory test results are listed in Table 8. It has been perceived that from Table 9, predicted results from the developed models are close to the experimental values. The percentage of prediction error is calculated by the following equation (given in Eq. 12) and the results are given in Table 9.

$$\text{Percentage of prediction error (\%)} = \left| \frac{\text{Exp. result} - \text{Pred. result}}{\text{Exp. result}} \right| \times 100 \tag{12}$$

8 Objective weight calculation using entropy method

The objective weight of the responses is calculated by the entropy weight method (EWM). In this technique, probability theory is used to estimate the degree of uncertainty (entropy) present in the response. It determines the significance of each response without considering the decider’s personal preferences. In this method, first goal is to set the decision matrix and then normalized the decision matrix. Secondly, response probability and degree of divergence i.e. average information contained in each response are calculated. Finally, entropy weights of the responses are determined. Steps to calculate the objective weights are given as follows:

Table 8 Confirmatory test results

Process parameters				Responses (Exp. result)			
T _{on}	T _{off}	S _v	W _t	V _c	D _v	R _a	δ
0.1	25	20	0.5	1.01	0.139	2.661	16
0.1	35	20	1.1	1.03	0.118	3.368	13
0.4	15	20	0.8	3.67	0.181	2.415	25
0.4	35	30	1.1	2.21	0.161	4.403	19
0.7	15	30	0.5	5.14	0.248	2.679	31
0.7	35	40	1.1	4.59	0.215	4.722	28

Table 9 Percentage of prediction error

Exp. Results				Pred. Results				% Pred. Error			
V _c	D _v	R _a	δ	V _c	D _v	R _a	δ	V _c	D _v	R _a	δ
1.01	0.139	2.661	16	0.98	0.144	2.678	17	2.97	3.60	0.64	6.25
1.03	0.118	3.368	13	0.96	0.112	3.388	12	6.80	5.08	0.59	7.69
3.67	0.181	2.415	25	3.70	0.189	2.409	26	0.82	4.42	0.25	4.00
2.21	0.161	4.403	19	2.15	0.154	4.421	18	2.71	4.35	0.41	5.26
5.14	0.248	2.679	31	5.29	0.259	2.650	30	2.92	4.44	1.08	3.23
4.59	0.215	4.722	28	4.63	0.225	4.747	27	0.87	4.65	0.53	3.57

Step-1 Objective identification.

Responses are assigned in the design table to complete the design matrix. In this study, two types of response are considered for analysis. First one is the ‘higher the better’ i.e. maximization type and the second one is the ‘lower the better’ kind of response i.e. minimization type. These responses are called "objectives" in EWM. In this case, cutting velocity is considered as ‘higher the better’ kind of problem and diagonal dimensional deviation, surface roughness and radial overcut are considered as ‘lower the better’ kind of problem [46–48].

Step-2 Decision matrix formation.

The template of the decision matrix is shown in Eq. 13. Responses are assigned in the column and experimental runs are represent in the row.

$$D_m = \begin{bmatrix} a_{1,1} & a_{1,2} & a_{1,3} & a_{1,4} \\ a_{2,1} & a_{2,2} & a_{2,3} & a_{2,4} \\ \dots & \dots & \dots & \dots \\ a_{26,1} & a_{26,2} & a_{26,3} & a_{26,4} \\ a_{27,1} & a_{27,2} & a_{27,3} & a_{27,4} \end{bmatrix} \tag{13}$$

Above expression (Eq. 13) is for (m × n) decision matrix, where m is the number of experimental run (m = 1, 2 26, 27) and n is the number of responses (n = 1, 2 4). a_{1,1}, a_{2,2} a_{i,j} are the elements in the matrix.

Step-3: Normalization of decision matrix.

Different responses have different dimensions. So, the several dimensional data is converted into dimensionless form using normalization technique. In EWM, following techniques are used to normalize the experimental data. It must be noted that the normalized decision matrix is always (N_{ij}) ∈ [0, 1].

$$N_{ij} = \frac{a_{ij}}{\text{Maximum}(a_{ij})} \tag{14}$$

$$N_{ij} = \frac{\text{Minimum}(a_{ij})}{a_{ij}} \tag{15}$$

The above two equations (Eqs. 14&15) are used to normalized the experimental data. Generally, Eq. 14 is used for beneficial type i.e. for maximization problem (Here, V_c) whereas Eq. 15 is used for non-beneficial type i.e. minimization problem (Here, D_v, R_a and δ).

Step-4 Response probability.

Probability of the response (P_{ij}) is used to find the entropy value. The following equation (Eq. 16) is used to calculate the probability of a response.

$$P_{ij} = \frac{N_{ij}}{\sum_{i=1}^n N_{ij}} \tag{16}$$

Step-5 Entropy measurement.

Table 10 Result obtained from entropy analysis

Sl. no.	Calculations	V _c	D _v	R _a	δ
1	$\sum_{i=1}^n \{P_{ij} \log_e(P_{ij})\}$	- 1.3577	- 1.4199	- 1.3904	- 1.4087
2	$\frac{1}{\log_e(y)}$	0.6986			
3	$-X \sum_{i=1}^n \{P_{ij} \log_e(P_{ij})\}$	0.9485	0.9920	0.9713	0.9842
4	$ 1 - E_j $	0.0514	0.0080	0.0286	0.0158
5	$\sum_{j=1}^m d_v$	0.1038			
6	w _j	0.4951	0.0770	0.2756	0.1521
7	Weight (%)	49.52	7.71	27.56	15.21
8	Annotations (weight)	w ₁	w ₂	w ₃	w ₄

Entropy of response is calculated by using following equation (Eq. 17).

$$E_j = -X * \sum_{i=1}^n \{P_{ij} \log_e(P_{ij})\} \quad (0 \leq E_j \leq 1) \quad (17)$$

where $X = \frac{1}{\log_e(y)}$; y is the number of experimental runs (y = 27) and E_j is entropy.

Step-6 Degree of divergence calculation.

Degree of divergence (d_v) is calculated by using following equation.

$$d_v = |1 - E_j| \quad (18)$$

Step-7 Entropy weight.

Entropy weight is calculated after finding the degree of divergence. Following equation is used to calculate the entropy weight.

$$w_j = \frac{d_v}{\sum_{j=1}^m d_v} \quad (19)$$

Table 10 shows the entropy weight calculation results. In this case, value of m and n are 27 and 4 respectively. Entropy value for cutting velocity (V_c), diagonal dimensional deviation (D_v), surface roughness (R_a) and radial overcut (δ) are 0.9485, 0.9920, 0.9713 and 0.9842. The corresponding entropy weight of V_c, D_v, R_a and δ are obtained as w₁ = 0.4951, w₂ = 0.0770, w₃ = 0.2756 and w₄ = 0.1521 respectively.

9 Searching optimal solution using weight based constrained Pareto algorithm

To search the Pareto optimal solutions, objective function is formulated as follows:

$$\text{Objective function; } g(x) = w_i \times y(x) \quad (20)$$

where g(x) defined as weight assigned objective function of cutting velocity (V_c), diagonal dimensional deviation (D_v), surface roughness (R_a) and radial overcut (δ). w_i is the weight of response (i = 1, 2, 3 ...).

Diagonal dimensional deviation, surface roughness and radial overcut are conflicting in nature with cutting velocity. Therefore, it is impossible to make a potential optimal solution by conventional optimization technique that can gives minimum D_v or R_a and maximum V_c simultaneously. To handle such problem efficiently, weight based constrained Pareto algorithm is used. In this process, a single objective is consider to optimize and other objective is consider as constraints. To enhance the production rate, it is better strategy to select an appropriate parameter setting that can give the maximum cutting velocity, while maintaining the surface roughness and diagonal dimensional deviation within desired limit. In this case, cutting velocity is selected as an objective function that is to be maximized whereas D_v and R_a both are considered as constraints. The constrained optimization problem is expressed as follows (Shown in Eq. 21):

$$\text{Maximum cutting velocity}(V_c) = f(T_{on}, T_{off}, S_v, W_t) \quad (21)$$

Subjected to D_v ≤ α (within desired limit).

where 0.1 ≤ T_{on} ≤ 0.7 15 ≤ T_{off} ≤ 35 20 ≤ S_v ≤ 40 0.5 ≤ W_t ≤ 1.1

Here α is the maximum allowable diagonal dimensional deviation. The value of α is within the predicted diagonal dimensional deviation (D_v) values, i.e. between 0.128 and 0.241 mm. For an example, if the required diagonal dimensional deviation is ≤ 0.202 mm, then the best parameter combination is T_{on} = 0.4 μs, T_{off} = 25 μs, S_v = 33 V & W_t = 1.1 kg. This combination gives a cutting velocity of 3.04 mm/min, while maintaining the diagonal dimensional deviation within 0.202 mm. Now if the required surface roughness is less than or equal to 1.764 μm then the aforementioned parameter settings is not appropriate. For that

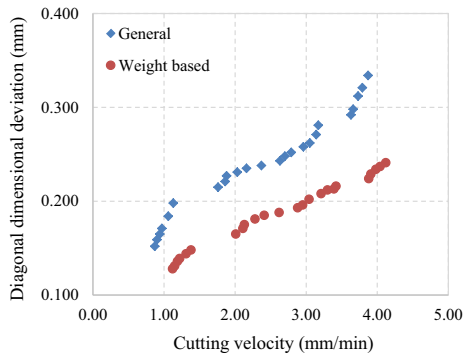


Fig. 6 Pareto optimal plot of cutting velocity vs. Diagonal dimensional deviation

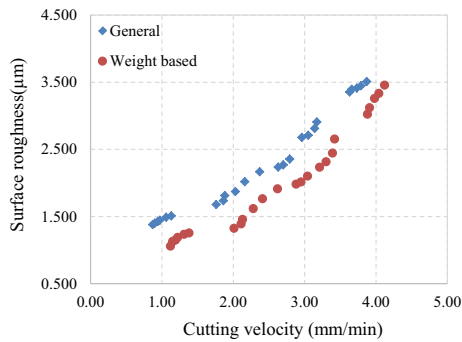


Fig. 7 Pareto optimal plot of Cutting velocity vs. Surface roughness

purpose, best parameter settings to obtained the required surface finish is $T_{on} = 0.3 \mu s$, $T_{off} = 35 \mu s$, $S_v = 40 V$ & $W_t = 0.6 kg$. Now, cutting velocity obtained in this parameter setting (i.e. $T_{on} = 0.3 \mu s$, $T_{off} = 35 \mu s$, $S_v = 40 V$ and $W_t = 0.6 kg$), is 2.41 mm/min. Here two different cutting velocities are obtained from two different set of parametric combinations. So, it is a challenging task to select which parameter settings is to be the best for machining. In single pass cutting (rough-cut) operation, cutting velocity is a prime important factor that determine the productivity. Therefore, 3.04 mm/min cutting velocity is always preferable than 2.41 mm/min when productivity is vital. In this case, 3.04 mm/min cutting velocity crosses the allowable surface roughness limit (i.e. $R_a = 1.764 \mu m$) while maintaining diagonal dimensional deviation within 0.202 mm. So, it is a better strategy to machine at lower cutting speed to maintain the accuracy and surface finish within desired limit in rough cutting operation.

A MATLAB programme is developed to find the Pareto optimal solution for cutting velocity, diagonal dimensional deviation and surface roughness. Total 24 numbers of optimal solutions are obtained by executing the developed MATLAB programme. General and weight based Pareto optimal results are plotted in the Figs. 6 and 7. For convenience, cutting velocity is considered along the X-axis whereas diagonal

dimensional deviation and surface roughness are considered along the Y-axis. It is observed that from the Figs. 6 and 7, weight-based Pareto results are better than the General Pareto results. In this case, minimum diagonal dimensional deviation obtained by General Pareto algorithm is 0.152 mm whereas weight-based result is 0.128 mm. Similarly, weight-based solution of surface roughness is $1.058 \mu m$ whereas General solution is $1.379 \mu m$ for a given cutting velocity of 1.12 mm/min. This Pareto optimal solution can be use as instruction manual for manufacturing engineer. Just by scanning the optimal chart, anybody can select an appropriate parametric combination for a given diagonal dimensional deviation and surface roughness requirement. Table 11 comprises an organize list of all weight-based Pareto optimal solutions. It may be pointed out that the radial overcut is not considered as an objective function in optimization. The radial overcut can be eliminated by adjusting the wire offset value during machining. So, measurement and prediction of radial overcut is important.

10 Surface roughness and surface topography analysis

In WEDM, surface roughness is determined by the size of spark crater generated during machining. The generation of spark crater is determined by the discharge power. This discharge power is controlled by pulse and voltage parameter settings while machining [23]. High discharge power i.e. high pulse parameter setting, causes violent sparks and generates impulsive forces; as a result, craters, deep holes, straits and nuggets are formed in the machined surface (shown in Fig. 8a, b) [34, 37]. Previously mentioned uneven fusing structures and surface irregularities are increases as the discharge power per pulse increases. SJ 410 contact type roughness tester is used to measure the surface roughness value and the CCI microscope is used to observe the surface topography of the machined surface. Deep holes and discharge craters are shallow in low pulse parameter settings, whereas these becomes wider and deeper when pulse parameter setting is increases to the higher side.

11 Microstructure and EDS analysis

After WEDM operation, work-specimen is placed under a scanning electron microscope to observe microstructural changes that occurred in the machined surface. Figure 9a, b shows the SEM micrograph of Al 7075 workpiece after machining. This micrograph reveals that the machined surface is full of craters, recast globules and solidified materials. Molten materials formed the recast globules after cooling. It creates pulp-like structures entire the machined surface.

Table 11 Pareto optimal chart for Al 7075

Sl. no.	T_{on} (μs)	T_{off} (μs)	S_v (volt)	W_t (kg)	V_c (mm/min)	D_v (mm)	R_a (μm)
1	0.1	35	33	0.5	1.12	0.128	1.058
2	0.1	35	33	0.5	1.15	0.131	1.129
3	0.1	35	40	0.5	1.19	0.136	1.148
4	0.1	35	40	0.5	1.22	0.139	1.189
5	0.1	25	24	1.1	1.31	0.144	1.234
6	0.2	25	24	0.5	1.38	0.148	1.254
7	0.2	35	32	1.1	2.01	0.165	1.324
8	0.2	35	30	0.8	2.11	0.171	1.389
9	0.3	35	40	0.5	2.13	0.175	1.456
10	0.3	35	40	0.6	2.28	0.181	1.617
11	0.3	35	40	0.6	2.41	0.185	1.764
12	0.3	25	20	0.8	2.62	0.188	1.912
13	0.4	35	33	0.6	2.88	0.193	1.981
14	0.4	25	33	0.7	2.95	0.196	2.014
15	0.4	25	33	1.1	3.04	0.202	2.101
16	0.5	25	40	0.5	3.21	0.208	2.233
17	0.5	35	40	0.6	3.30	0.212	2.315
18	0.6	35	33	0.5	3.39	0.213	2.445
19	0.6	35	40	0.6	3.42	0.216	2.654
20	0.7	35	40	0.5	3.88	0.224	3.024
21	0.7	35	40	0.6	3.91	0.229	3.121
22	0.7	35	40	0.6	3.98	0.234	3.258
23	0.7	16	40	0.6	4.04	0.237	3.334
24	0.7	16	40	1.1	4.12	0.241	3.457

These surface irregularities are more pronounced when the pulse duration and servo voltage is increased. As the pulse discharge and voltage are turned up, high intensity of pulse discharge hits the workpiece harder that causes aggressive erosion and make the surface rougher.

Energy dispersive spectroscopy (EDS) of the machined surface is carried out to observe how the composition is altered in WEDM operation. Figure 9a-b shows the EDS pattern of the machined surface. It is observed that copper (Cu), manganese (Mn) and zinc (Zn) are detected on the Al 7075 surface. These are deposited due to the melting and deposition of wire electrodes on the workpiece. However, foreign element like oxygen (O) is also detected on the machined surface; this is happening due to the dielectric fluid that contains oxygen (O) [49]. During machining, dielectric fluid (deionized water) decomposes into hydrogen and oxygen. Oxygen is released owing to the disassociation of dielectric fluid (deionized water) at very high temperatures [50]. This oxygen at high temperatures may result in oxidation on the machined surface [51]. This could cause more porous surfaces in the machined areas and therefore decreases the hardness and fracture toughness of the machined surfaces.

12 Conclusions

The present work proposed an integrated approach of entropy-weight multi-constrained optimization in WEDM of Al 7075 alloy. Four important responses, such as cutting velocity (V_c), diagonal dimensional deviation (D_v), surface roughness (R_a) and radial overcut (δ) are considered to evaluate the performance characteristics of the process. The entropy weight method (EWM) is introduced to find the appropriate weight of the objective and constrained Pareto algorithm is used to establish systematic trade-off of the process. The conclusions of the present work are summarized as follows:

- Single-pass cutting in WEDM of Al 7075 has been experimentally investigated in this study. An experimental result shows that the Al 7075 alloy has been effectively machined with a considerably high cutting velocity of 5.88 mm/min. The minimum diagonal dimensional deviation and radial overcut values that are obtained during experimentation are 0.123 mm and 11 μm whereas the minimum surface roughness is 1.237 μm .

Fig. 8 Surface roughness profile and surface topography of the machined surface **a** $T_{on} = 0.1 \mu s$, **b** $T_{on} = 0.7 \mu s$

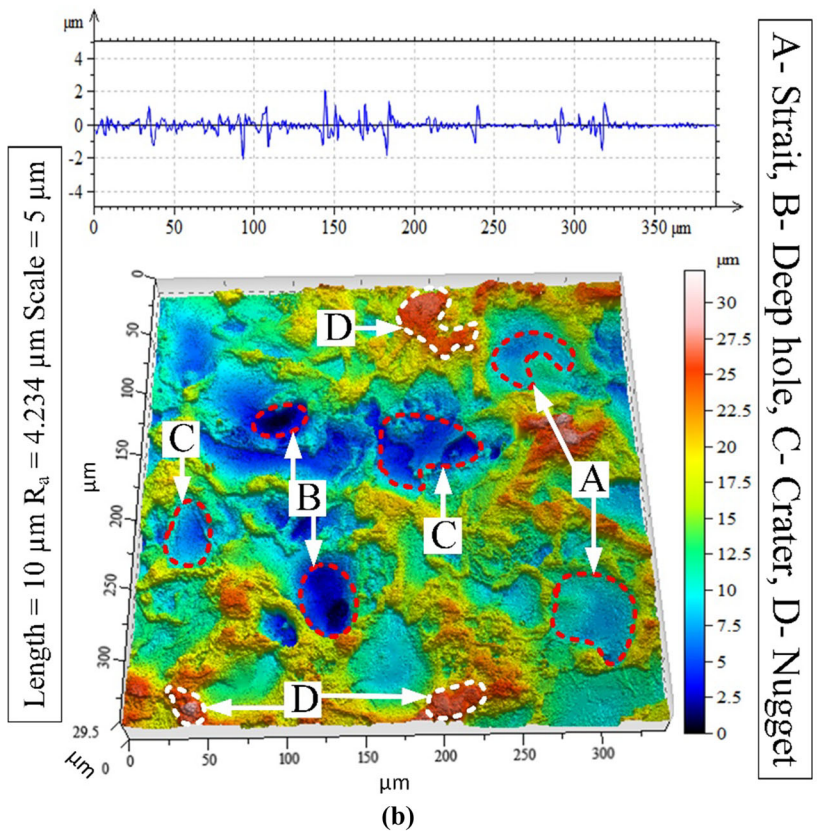
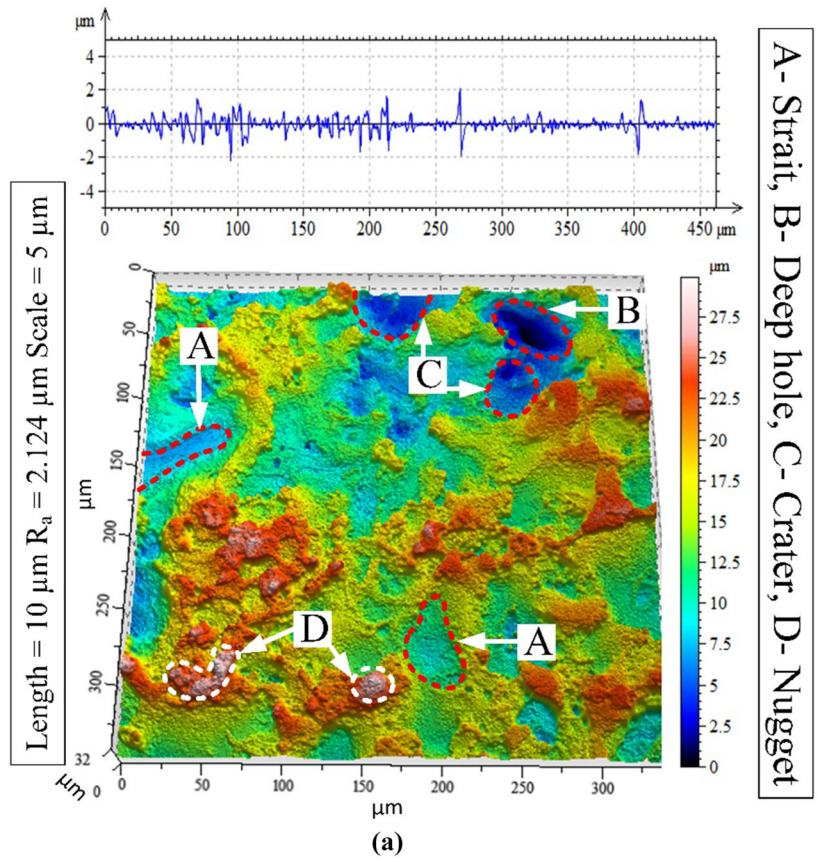
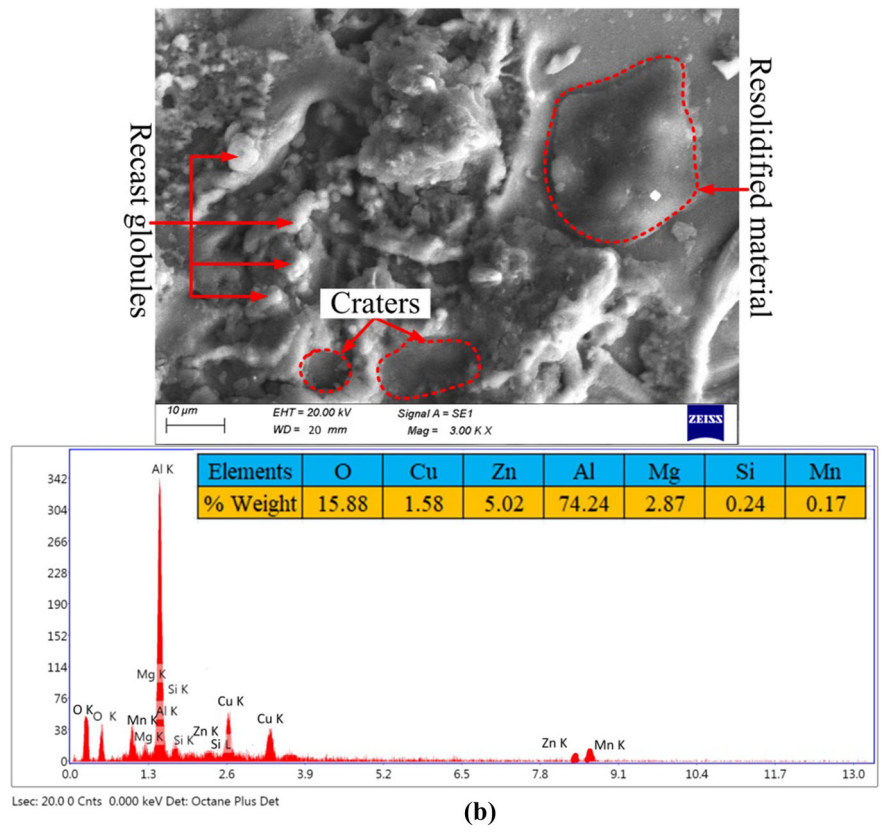
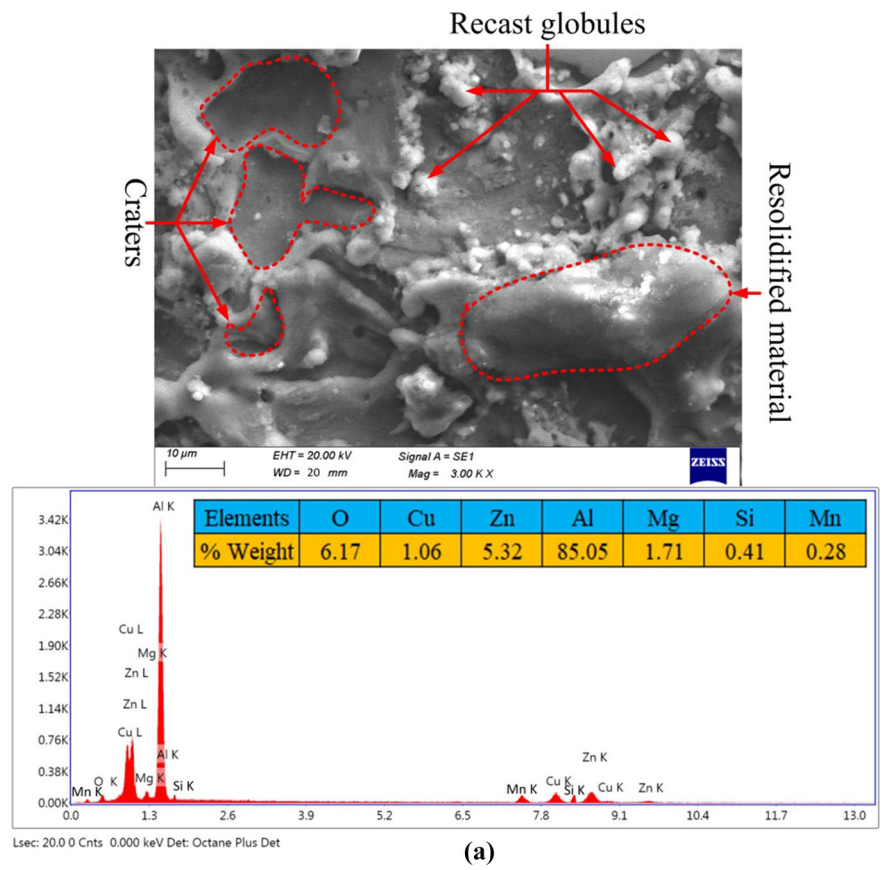


Fig. 9 SEM micrograph and EDS pattern of the machined surface
a $T_{on} = 0.1 \mu s$, **b** $T_{on} = 0.7 \mu s$



- ANOVA result reveals that pulse duration (T_{on}) and pulse interval (T_{off}) are found major dominating factors to determine the cutting velocity (V_c), diagonal dimensional deviation (D_v), surface roughness (R_a) and radial overcut (δ) whereas servo voltage has moderate impact on all responses. On the other hand, wire tension have major impact on diagonal dimensional deviation and overcut. From the main effect plot of S/N ratio of wire tension, it is observed that increasing wire tension (W_t) gives the best accuracy (diagonal) and the least overcut (radial).
- Objective weights obtained by the entropy method are 0.4951(w_1) for cutting velocity, 0.0770(w_2) for diagonal dimensional deviation, 0.2756(w_3) for surface roughness and 0.1521(w_4) for radial overcut.
- It is found that using weight-base optimization technique, for a broad range of cutting velocity, diagonal dimensional deviation is varied from 0.128 to 0.241 mm and surface roughness is varied from 1.058 to 3.457 μm .
- Weight-based optimal solutions are more significant than general Pareto solutions. It is found that the average cutting velocity, diagonal dimensional accuracy and surface finish are improved by 10.5%, 28.3% and 13.7%.
- Surface topography of the machined surface reveals that recast globules, redeposited materials and deep holes decrease as the pulse duration decreases and the pulse interval increases. It is observed that foreign elements like copper and oxygen deposition increase with the increase in pulse duration.

The present work is extremely useful to maximize the productivity while maintaining the diagonal dimensional deviation and surface roughness within a required limit. An optimal chart prepared by the Pareto algorithm will be helpful for effective machining of Al 7075 alloy. Different advanced manufacturing and production industries can use these results to complete precise jobs more quickly.

Acknowledgements The author(s) acknowledge the assistance provided by the CAS-V program of the Production Engineering Department, Jadavpur University under UGC.

Funding The author(s) received no financial support for the research from any profit or non-profit organization.

Declarations

Conflict of interest The author(s) declared no potential conflicts of interest with respect to the research, authorship, and/or publication of this article.

References

1. Gunen, A., Ceritbinmez, F., Pate, K., et al.: WEDM machining of MoNbTaTiZr refractory high entropy alloy. *CIRP J. Manuf. Sci. Technol.* **38**, 547–559 (2022). <https://doi.org/10.1016/j.cirpj.2022.05.021>
2. Vora, J., Khanna, S., Chaudhari, R., et al.: Machining parameter optimization and experimental investigations of nano-graphene mixed electrical discharge machining of nitinol shape memory alloy. *J. Market. Res.* **19**, 653–668 (2022). <https://doi.org/10.1016/j.jmrt.2022.05.076>
3. Sivaprakasam, P., Hariharan, P., Gowri, S.: Experimental investigations on nano powder mixed Micro-Wire EDM process of Inconel-718 alloy. *Measurement* **147**, 106844 (2019). <https://doi.org/10.1016/j.measurement.2019.07.072>
4. Tisza, M., Czinege, I.: Comparative study of the application of steels and aluminium in lightweight production of automotive parts. *Int. J. Lightw. Mater. Manuf.* **1**(4), 229–238 (2018). <https://doi.org/10.1016/j.ijlmm.2018.09.001>
5. Salvati, E., Korsunsky, A.M.: Micro-scale measurement & FEM modelling of residual stresses in AA6082-T6 Al alloy generated by wire EDM cutting. *J. Mater. Process. Technol.* **275**, 116373 (2020). <https://doi.org/10.1016/j.jmatprotec.2019.116373>
6. Liu, X., Xu, P., Zhao, J., et al.: Material machine learning for alloys: Applications, challenges and perspectives. *J. Alloys Compd.* **921**, 165984 (2022). <https://doi.org/10.1016/j.jallcom.2022.165984>
7. Najmon, J.C., Raeisi, S., Tovar, A.: Review of additive manufacturing technologies and applications in the aerospace industry. In: *Additive Manufacturing for the Aerospace Industry*, pp. 7–31 (2019). <https://doi.org/10.1016/B978-0-12-814062-8.00002-9>
8. Williams, J.C., Starke, E.A.: Progress in structural materials for aerospace systems. *Acta Mater.* **51**(19), 5775–5799 (2003). <https://doi.org/10.1016/j.actamat.2003.08.023>
9. Saravanan, R., Anbuezhayan, G., Mamidi, V.K., et al.: Optimizing WEDM parameters on nano-SiC-Gr reinforced aluminum composites using RSM. *Adv. Hybrid Compos. Eng. Appl.* (2022). <https://doi.org/10.1155/2022/1612539>
10. Suresh, S., Sudhakara, D.: Investigations on machining and wear characteristics of Al 7075/Nano-SiC composites with WEDM. *J. Bio Tribo Corros.* **5**, 99 (2019). <https://doi.org/10.1007/s40735-019-0293-x>
11. Xu, J., Qiu, R., Lian, Z., et al.: Wear and corrosion resistance of electroforming layer after WEDM for 7075 aluminum alloy. *Mater. Res. Express.* **5**(6), 066502 (2018). <https://doi.org/10.1088/2053-1591/aac636>
12. Dey, A., Pandey, K.M., et al.: Selection of optimal processing condition during WEDM of compocasted AA6061/cenosphere AMCs based on grey-based hybrid approach. *Mater. Manuf. Processes* **33**(14), 1549–1558 (2018). <https://doi.org/10.1080/10426914.2018.1453154>
13. Mandal, A., Dixit, A.R.: State of art in wire electrical discharge machining process and performance. *Int. J. Mach. Mach. Mater.* **16**(1), 1–21 (2014). <https://doi.org/10.1007/s00170-020-06218-5>
14. Kumar, K., Agarwal, S.: Multi-objective parametric optimization on machining with wire electric discharge machining. *Int. J. Adv. Manuf. Technol.* **62**, 617–633 (2012). <https://doi.org/10.1007/s00170-011-3833-1>
15. Panda, R.C., Sharada, A., Samanta, L.D.: A review on electrical discharge machining and its characterization. *Mater. Today Proc.* (2022). <https://doi.org/10.1016/j.matpr.2020.11.546>

16. Xie, B.C., Wang, Y.K., Wang, Z.L., et al.: Numerical simulation of titanium alloy machining in electric discharge machining process. *Trans. Nonferrous Metals Soc. China* **21**(2), 434–439 (2011). [https://doi.org/10.1016/S1003-6326\(11\)61620-8](https://doi.org/10.1016/S1003-6326(11)61620-8)
17. Kumar, A., Mandal, A., Dixit, A.R., et al.: Performance evaluation of Al₂O₃ nano powder mixed dielectric for electric discharge machining of Inconel 825. *Mater. Manuf. Process.* **33**(9), 986–995 (2018). <https://doi.org/10.1080/10426914.2017.1376081>
18. Yu, R.Z.Z., Yan, C., Li, J., et al.: Micro electrical discharge machining in nitrogen plasma jet. *Precis. Eng.* **51**, 198–207 (2018). <https://doi.org/10.1016/j.precisioneng.2017.08.011>
19. Mandal, A., Dixit, A.R., Chattopadhyay, S., et al.: Improvement of surface integrity of Nimonic C 263 super alloy produced by WEDM through various post-processing techniques. *Int. J. Adv. Manuf. Technol.* **93**, 433–443 (2017). <https://doi.org/10.1007/s00170-017-9993-x>
20. Varun, A., Venkaiah, N.: Simultaneous optimization of WEDM responses using grey relational analysis coupled with genetic algorithm while machining EN 353. *Int. J. Adv. Manuf. Technol.* **76**, 675–690 (2015). <https://doi.org/10.1007/s00170-014-6198-4>
21. Rao, T.B., Krishna, A.G.: Selection of optimal process parameters in WEDM while machining Al7075/SiCp metal matrix composites. *Int. J. Adv. Manuf. Technol.* **73**, 299–314 (2014). <https://doi.org/10.1007/s00170-014-5780-0>
22. Karthik, S., Prakash, K.S., Gopal, P.M., et al.: Influence of materials and machining parameters on WEDM of Al/AlCoCrFeNiMo_{0.5} MMC. *Mater. Manuf. Process.* **34**(7), 759–768 (2019). <https://doi.org/10.1080/10426914.2019.1594250>
23. Pujara, J., Kothari, K.D., Gohil, A.V.: Process parameter optimization for MRR and surface roughness during machining LM6 aluminum MMC on WEDM. *Adv. Eng. Forum* **20**, 42–50 (2017). <https://doi.org/10.4028/www.scientific.net/AEF.20.42>
24. Ishfaq, K., Anwar, S., Ali, M.A., et al.: Optimization of WEDM for precise machining of novel developed Al6061-7.5% SiC squeeze-casted composite. *Int. J. Adv. Manuf. Technol.* **111**, 2031–2049 (2020). <https://doi.org/10.1007/s00170-020-06218-5>
25. Ishfaq, K., Ahmed, N., Mufti, N.A., et al.: Exploring the contribution of unconventional parameters on spark gap formation and its minimization during WEDM of layered composite. *Int. J. Adv. Manuf. Technol.* **102**, 1659–1669 (2019). <https://doi.org/10.1007/s00170-019-03301-4>
26. Ishfaq, K., Ahmed, N.: WEDM of layered composite: analyzing material removal and cut quality issues. *Mater. Manuf. Process.* **34**(10), 1073–1082 (2019). <https://doi.org/10.1080/10426914.2019.1615083>
27. Ishfaq, K., Mufti, N.A., Mughal, M.P., et al.: Investigation of wire electric discharge machining of stainless-clad steel for optimization of cutting speed. *Int. J. Adv. Manuf. Technol.* **96**, 1429–1443 (2018). <https://doi.org/10.1007/s00170-018-1630-9>
28. Rao, R.V., Pawar, P.J.: Modelling and optimization of process parameters of wire electrical discharge machining. *Proc. Inst. Mech. Eng. Part B J. Eng. Manuf.* **223**(11), 1431–1440 (2009). <https://doi.org/10.1243/09544054JEM1559>
29. Darji, R.S., Joshi, G.R., Hembrom, S., et al.: Powder mixed electrical discharge machining of Inconel 718: investigation on material removal rate and surface roughness. *Int. J. Interact. Des. Manuf.* (2022). <https://doi.org/10.1007/s12008-022-01059-w>
30. Marashi, H., Jafarlou, D.M., et al.: State of the art in powder mixed dielectric for EDM applications. *Precis. Eng.* **46**, 11–33 (2016). <https://doi.org/10.1016/j.precisioneng.2016.05.010>
31. Rao, T.B.: Optimizing machining parameters of wire-EDM process to cut Al7075/SiCp composites using an integrated statistical approach. *Adv. Manuf.* **4**, 202–216 (2016). <https://doi.org/10.1007/s40436-016-0148-3>
32. Lal, S., Kumar, S., et al.: Multi-response optimization of wire electrical discharge machining process parameters for Al7075/Al₂O₃/SiC hybrid composite using Taguchi-based grey relational analysis. *Proc. Inst. Mech. Eng. Part B J. Eng. Manuf.* **229**(2), 229–237 (2015). <https://doi.org/10.1177/0954405414526382>
33. Aruri, D., Kolli, M., et al.: RSM-TOPSIS multi optimization of EDM factors for rotary stir casting hybrid (Al7075/B4C/Gr) composites. *Int. J. Interact. Des. Manuf.* (2022). <https://doi.org/10.1007/s12008-022-00893-2>
34. Mandal, K., Sekh, M., et al.: Influence of dielectric conductivity on corner error in wire electrical discharge machining of Al 7075 alloy. *Proc. Inst. Mech. Eng. C J. Mech. Eng. Sci.* **235**(20), 5043–5056 (2020). <https://doi.org/10.1177/0954406220978268>
35. Mandal, K., Bose, D., et al.: Experimental investigation of process parameters in WEDM of Al 7075 alloy. *Manuf. Rev.* **7**(30), 1–9 (2020). <https://doi.org/10.1051/mfreview/2020021>
36. Kuriachen, B., Somashekhar, K.P., Mathew, J.: Multi response optimization of micro-wire electrical discharge machining process. *Int. J. Adv. Manuf. Technol.* **76**, 91–104 (2015). <https://doi.org/10.1007/s00170-014-6005-2>
37. Ikram, A., Mufti, N.A., Saleem, M.Q., et al.: Parametric optimization for surface roughness, kerf and MRR in wire electrical discharge machining (WEDM) using Taguchi design of experiment. *J. Mech. Sci. Technol.* **27**, 2133–2141 (2013). <https://doi.org/10.1007/s12206-013-0526-8>
38. Thankachan, T., Prakash, K.S., Loganathan, M.: WEDM process parameter optimization of FSPed copper-BN composites. *Mater. Manuf. Process.* **33**(3), 350–358 (2018). <https://doi.org/10.1080/10426914.2017.1339311>
39. Priyadarshini, M., Vishwanatha, H.M., Biswas, C.K., et al.: Effect of grey relational optimization of process parameters on surface and tribological characteristics of annealed AISI P20 tool steel machined using wire EDM. *Int. J. Interact. Des. Manuf.* (2022). <https://doi.org/10.1007/s12008-022-00954-6>
40. Prakash, S., et al.: Investigation of mechanical and tribological characteristics of medical grade Ti₆Al₄V titanium alloy in addition with corrosion study for wire EDM process. *Adv. Mater. Sci. Eng.* (2022). <https://doi.org/10.1155/2022/5133610>
41. Kuriachen, B., Lijesh, K.P., Kuppan, P.: Multi response optimization and experimental investigations into the impact of wire EDM on the tribological properties of Ti–6Al–4V. *Trans. Indian Inst. Met.* **71**, 1331–1341 (2018). <https://doi.org/10.1007/s12666-017-1267-7>
42. Taguchi, G.: *Introduction to quality engineering: designing quality into products and processes.* Asian Productivity Organization, Tokyo (1990).
43. Singh, J., Singh, J.P.: Performance analysis of erosion resistant Mo₂C reinforced WC-CoCr coating for pump impeller with Taguchi's method. *Ind. Lubr. Tribol.* **74**(4), 431–441 (2022). <https://doi.org/10.1108/ilt-05-2020-0155>
44. Singh, J.: Tribo-performance analysis of HVOF sprayed 86WC-10Co4Cr & Ni-Cr₂O₃ on AISI 316L steel using DOE-ANN methodology. *Ind. Lubr. Tribol.* **73**(5), 727–735 (2021). <https://doi.org/10.1108/ilt-04-2020-0147>

45. Singh, J., Kumar, S., Singh, G.: Taguchi's approach for optimization of Tribo-resistance parameters for SS304. *Mater. Today Proc.* **5**(2), 5031–5038 (2018). <https://doi.org/10.1016/j.matpr.2017.12.081>
46. Jangra, K., Grover, S., Aggarwal, A.: Optimization of multi machining characteristics in WEDM of WC-5.3%Co composite using integrated approach of Taguchi, GRA and entropy method. *Front. Mech. Eng.* **7**, 288–299 (2012). <https://doi.org/10.1007/s11465-012-0333-4>
47. Abhilash, P.M., Chakradhar, D.: Multi-response optimization of wire EDM of Inconel 718 using a hybrid entropy weighted GRA-TOPSIS method. *Process Integr. Optim. Sustain.* **6**, 61–72 (2022). <https://doi.org/10.1007/s41660-021-00202-6>
48. Kumar, B.K., Das, V.C.: Study and parameter optimization with AISI P20+Ni in wire EDM performance using RSM and hybrid DBN based SAR. *Int. J. Interact. Des. Manuf.* (2022). <https://doi.org/10.1007/s12008-022-00991-1>
49. Kumar, S., Grover, S., Walia, R.S.: Residual stresses and surface topography investigation of AISI D3 tool steel under of ultrasonic vibration assisted wire-EDM. *Int. J. Interact. Des. Manuf.* **16**, 1417–1438 (2022). <https://doi.org/10.1007/s12008-022-01034-5>
50. Chaudhari, R., Vora, J.J., Maniprabu, S.S., et al.: Pareto optimization of WEDM process parameters for machining a NiTi shape memory alloy using a combined approach of RSM and heat transfer search algorithm. *Adv. Manuf.* **9**, 64–80 (2021). <https://doi.org/10.1007/s40436-019-00267-0>
51. Kumar, A., Gorver, N., et al.: Investigating the influence of WEDM process parameters in machining of hybrid aluminum composites. *Adv. Compos. Lett.* (2020). <https://doi.org/10.1177/2633366X2096313>

Publisher's Note Springer Nature remains neutral with regard to jurisdictional claims in published maps and institutional affiliations.

Springer Nature or its licensor (e.g. a society or other partner) holds exclusive rights to this article under a publishing agreement with the author(s) or other rightsholder(s); author self-archiving of the accepted manuscript version of this article is solely governed by the terms of such publishing agreement and applicable law.